SolarPACES 2024, 30th International Conference on Concentrating Solar Power, Thermal, and Chemical Energy Systems

Solar Industrial Process Heat and Thermal Desalination

https://doi.org/10.52825/solarpaces.v3i.2455

Published: 22 Sep. 2025

Precalciner Geometry Optimization Considering H_2O and CO_2 Heat Transfer Fluid for Cement Production

Javier Martell[1,*], Brantley Mills[1], and Nathan Schroeder[1]

[1]Sandia National Laboratories, US

*Correspondence: Javier Martell, jamarte@sandia.gov

Abstract. The cement industry accounts for 3 – 5% of global CO_2 emissions and is difficult to decarbonize due to the high temperature used in the process. The cement raw material requires temperatures up to 900 °C for calcination and 1500 °C for sintering. Synhelion has developed an absorbing-gas solar receiver which can provide 1500 °C heat to the process via an H_2O/CO_2 heat transfer fluid to provide fossil-free heating for the preheating and calcination stages. However, very little work has been done to investigate the viability of solar-heated H_2O and CO_2 gases to efficiently calcine the cement raw meal relative to conventional gas-fired precalciners. The objective of this study is to present an optimized small scale precalciner considering particle suspension, flow dynamics, heat transfer, and thermochemistry of the raw meal when using H_2O and CO_2 gases. The optimization of the precalciner geometry using a CFD model developed in ANSYS is presented.

Keywords: Precalciner Optimization, Fossil-Free Eating, Calcination

1. Introduction

Conventional cement production contributes ~3 – 5% of global carbon dioxide (CO2) emissions [1] and ~8% of anthropogenic CO2 emissions [2]. About 60% of CO2 emissions results from the release of CO2 during calcination of calcium carbonate (CaCO3), ~30% results from burning of fossil fuels to supply heat for the highly endothermic reaction, and ~10% results from indirect energy needs (e.g., electricity and transportation) [2]. Cement has been in use by humans throughout history; variations of the material were used up to 12,000 years ago, with the earliest archaeological discovery of consolidated whitewashed floor made from burned limestone and clay found in modern-day turkey [3]. While the use of cement in concrete has a very long history, the industrial production of cements started in the middle of the 19th century, first with shaft kilns then rotary kilns which became the standard equipment worldwide. Emissions from cement production have increased massively since the 1960s and have more than doubled since the turn of the century. More than four billion metric tons of cement are currently produced worldwide each year. In 2022, Global emissions from the manufacture of cement stood at 1.6 billion metric tons of carbon dioxide ($MtCO_2$) [4]. The conceptual layout of a modern cement production plant is presented in Figure 1. The production of cement involves the raw material (meal) preparation followed by the pyro-processing steps including the calcination of the material in calcination vessel at 900 °C and sintering in the rotary kiln at approximately 1500 ◦C to produce clinker. The heat required for raw meal pyro-processing is provided most commonly by combustion of coal and petcoke mix. The hot flue gases are used to pre-heat the raw materials and then treated in a Selective Catalytic Reduction (SCR) unit for NOx removal [5].

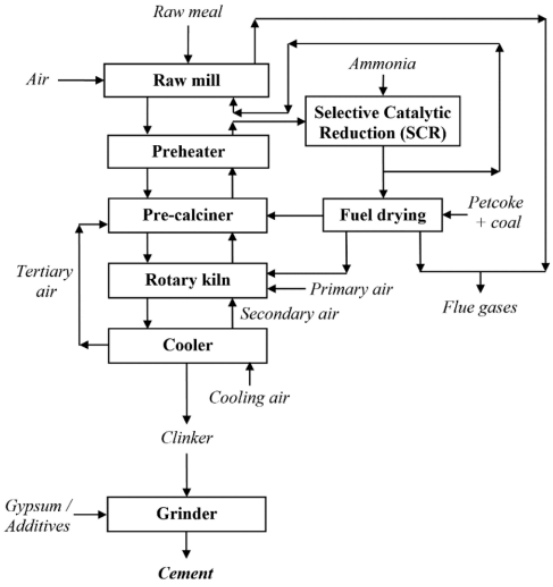

Figure 1. *Conventional cement production system layout [6].*

Over 80% of the energy required for calcination and clinkerization is in the preheaters and precalciner [7]. To move away from the conventional fossil fuel heating approach, Synhelion has developed an absorbing-gas solar receiver which can provide 1500 ℃ heat to the process via an H_2O/CO_2 heat transfer fluid. Figure 2 shows a schematic of Synhelion's receiver used to generate high-temperature (~1500 °C) heat for solar-driven pyro-processing of cement clinker [8]. Mixtures of superheated steam and CO_2 are passed through the receiver and volumetrically heated by thermal radiation from the irradiated walls of the blackbody-like cavity receiver. The hot gas can be delivered to the precalciner to calciner to drive off mineralized CO_2 from the calcium carbonite feedstock ($CaCO_3 \rightarrow CaO + CO_2$).

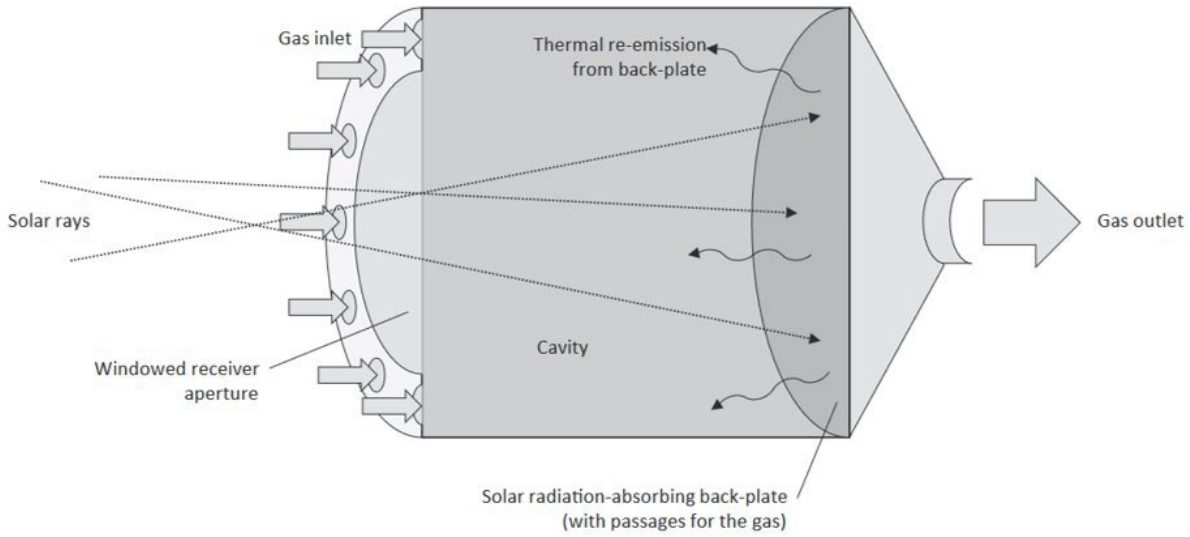

Figure 2. *Synhelion receiver schematic.*

Sandia, Synhelion, and Cemex intend to characterize and optimize particle suspension, particle and gas compositions, and thermochemical reactions associated with solar-thermal calcination in cyclonic preheaters and precalciners using CO_2 and/or H_2O as the heat-transfer fluid (HTF). The models and tests will de-risk and optimize designs for solar-thermal calcination

(including energy storage for continuous operation) to significantly reduce CO_2 emissions during cement production. The optimization of the precalciner geometry using a CFD model developed in ANSYS is presented.

2. Methods

2.1 Precalciner Geometry

Cement raw material is calcined with the precalciner vessel located upstream of the kiln where fuel combustion, heat exchangers, and decarbonation takes place. In existing precalciner vessels, fuel is added and combusted together with the cement raw material suspension. The raw material falls to the base of the calciner to enter the kiln while the combustion gases flow upward into the preheater tower where heat is transferred to the raw material. The cement raw meal is heated to 820-900 °C within the calciner to liberate the majority, 95%, of the CO_2 from mineral [9]. Figure 3 shows the standard industrial precalciner structure.

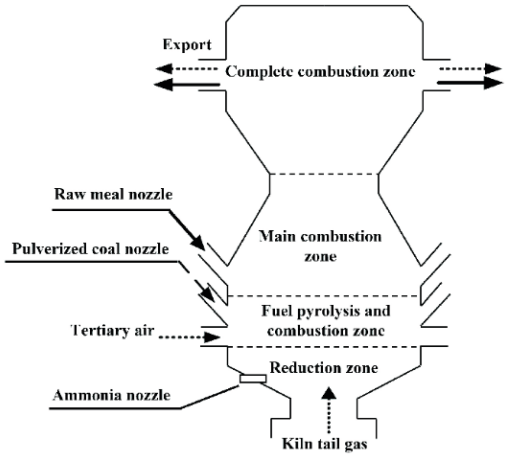

Figure 3. *Precalciner structure in industrial operations [9].*

Heat-transfer in a system using a H_2O/CO_2 HTF needs to be evaluated to ensure uniform heating of raw materials and calcination reactions. The current system being developed is a small-scale system that will be used to validate the CFD models. A commercial scale system will be modelled once the small-scale system experiment has validated the inputs to the CFD models. The study conducted here is simply ensuring that we can efficiently react the material at small scale. The proposed geometry needs to yield the most efficient calcination of raw meal possible to ensure commercial viability by maximizing residence time and calcination of the particles. The proposed geometry in figure 4 keeps a commercial cylindrical shape but uses a slightly different approach to introduce the raw meal and the hot greenhouse gases. The geometry uses a counterflow configuration in which particles are dropped with gravity against a counterflowing H_2O/CO_2 stream. The insertion of the raw meal occurs in the top centre of the cavity, while the H_2O/CO_2 stream enters the system at the opposite side flowing annularly along the reactor walls to help minimize contact with the walls and reduce entrainment. An expanding volume was added below the cavity to separate the particles from the entrained gas stream for sampling.

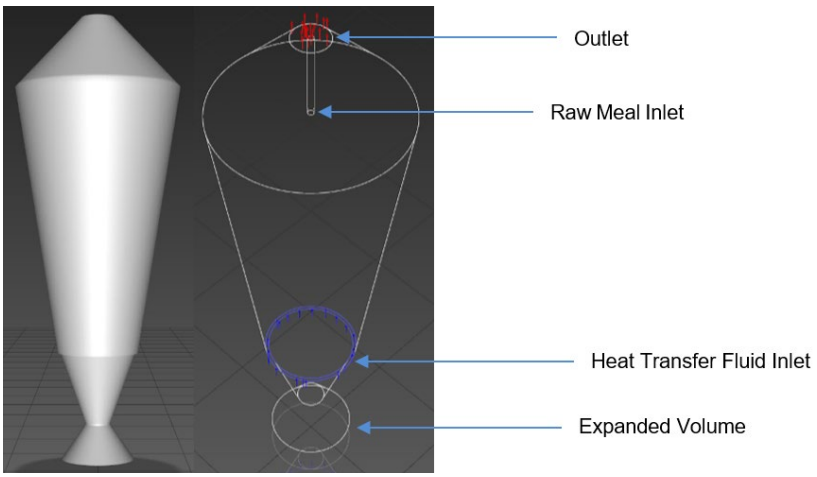

Figure 4. *Precalciner proposed geometry.*

2.2 Latin Hypercube Sampling Study

The purpose of this study is to design and optimize a small scale precalciner. The Dakota software package [10] was selected to govern the optimization process. Dakota is an open-source toolkit developed at Sandia National Labs that provides a framework for optimization, uncertainty quantification, parameters estimation, and sensitivity/variance analysis. It was chosen primarily for its flexibility in coupling with other simulation codes and its robust library of existing optimization routines and sampling strategies.

A Latin hypercube Sampling (LHS) study was developed to generate several geometric variations. The study was set to run a total of 184 samples with the variables outlined in table 1. Using the meshing scripts described in section 2.3, each geometric variation was generated and meshed. Then, each geometric realization was simulated using the CFD model in parallel. The incremental LHS approach was pursued. The study started with a small number of samples, and more were added in stages. As more samples were added, the statistical results were being monitored to see if they became more consistent. This helped to ensure a sufficient number of samples were produced for optimization.

Table 1. *Geometric variables for LHS study.*

Variable	Lower bound	Upper bound
Molar mass flow (mol/s)	0.15	0.30
Mass fraction	0	1
Center Height (mm)	500	2000
Center Slope (mm)	0	20
Center diameter (mm)	250	1500
Inlet thickness (mm)	25	50
Bottom cone height (mm)	200	400

A post-processor script was written in python to compare and rank all cases. The post-processor took the particles ID, x, y, z positions, residence time, calcination rate, and temperature data for 10,000 discrete phase model steps from each Fluent case. This data was used to calculate the mean residence time, calcination rate, temperature and fraction exited. The fraction exited refers to the number of particles that reached the bottom of the precalciner. This valued was calculated by taking the y position of the particles from fluent and specifying in the post-processor the y position of the bottom wall of the precalciner. By doing this, all the particles that had its y position value equal to the y position of the bottom wall would be counted as exiting the geometry.

2.3 CFD Model

To model the various geometries, a script was developed using the meshing software Cubit to reliably construct and mesh each variation. Examples of the geometries produced by this script are shown in figure 5. Consistent mesh sizes were used for the domain, and five boundary conditions added: 'meal stream" for particles injection, "outlet" for particles to exit the geometry, "inlet" for the H_2O/CO_2 stream, "kiln stream", and "walls". While this doesn't guarantee an appropriate spatial discretization for a given simulation, it was assumed that those simulations with inadequate meshes wouldn't affect the global trends significantly.

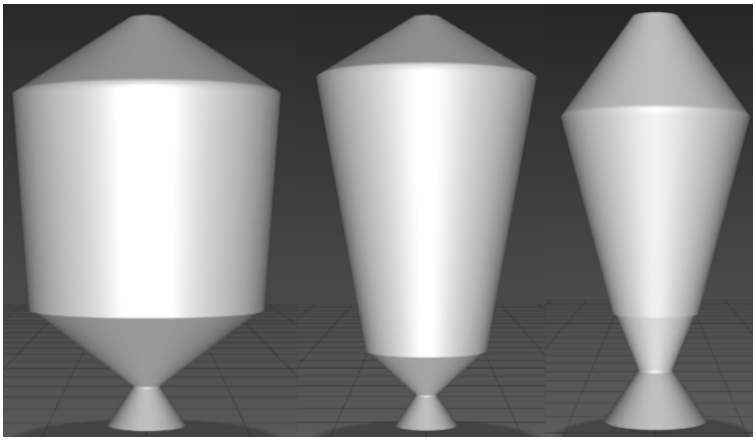

Figure 5. *Examples of precalciner geometries created by meshing script.*

The CFD model was developed using ANSYS Fluent. The model utilizes the energy equation (1) to simulate the heat transfer between the fluid flows. The realizable k-epsilon turbulence model with scalable wall function was utilized to simulate the flow. This turbulence model provides better accuracy for particular flow regimes including those involving strong streamline curvature, vortices, and rotation. The model consists of two transport equations: one for the turbulent kinetic energy (2) and one for the turbulent dissipation rate (3). The term "realizable" means that the model satisfies certain mathematical constraints on the Reynolds stresses, consistent with the physics of turbulent flows. This ensures that the predicted turbulent kinetic energy and dissipation rate are physically realistic. The scalable wall function is designed to improve the robustness and accuracy of simulations involving turbulent flows near walls, especially when dealing with coarse meshes or complex geometries ensuring the wall treatment remains valid and effective regardless of the near-wall mesh resolution. Radiation was modeled using the Discrete Ordinates (DO) radiation model. This radiation model solves the radiative transfer equation (4) for a finite number of discrete solid angles, each associated with a vector direction fixed in the global Cartesian system. To calculate the absorption coefficients, the weighted sum of grey gases model (WSGGM) is implemented. The WSGGM model is a reasonable compromise between the over simplified gray gas model and a complete model which considers particular absorption bands. The species transport model is used to model the chemistry between the H_2O/CO_2 gas and the raw meal particles. The transport equation for the mass fraction is given by equation (5). The Arrhenius rate law is used to model the reaction kinetics in the model. This law is based on the Arrhenius equation, which describes how the rate constant of a reaction varies with temperature. The pre-exponential factor and activation energy used are $1.0.10^{05}$, and $1.617.10^{08}$ respectively. Equation (6) shows the general form of the Arrhenius equation. The Discrete Phase Model (DPM) is used to simulate the raw meal particles in the system. The particle mean diameter for this study is $3.5.10^{-05}$ m. The trajectory of a discrete phase particle is determined by integrating the force balance on the particle as shown in equation (7).

$$\frac{\partial(\rho E)}{\partial t} + \nabla \cdot (\rho v E) = \nabla \cdot \left(k_{eff} \nabla T\right) + S_E \quad (1)$$

$$\frac{\partial(\rho k)}{\partial t} + \nabla \cdot (\rho v k) = \nabla \cdot \left(\frac{\mu_t}{\sigma_k} \nabla k\right) + G_k + G_b - \rho\epsilon - Y_M + S_k \quad (2)$$

$$\frac{\partial(\rho \epsilon)}{\partial t} + \nabla \cdot (\rho v \epsilon) = \nabla \cdot \left(\frac{\mu_t}{\sigma_\epsilon} \nabla_\epsilon\right) + \rho C_1 S_\epsilon - \rho C_2 \frac{\epsilon^2}{k+\sqrt{\nu\epsilon}} + C_1 \frac{\epsilon}{k} C_3 \rho G_b + S_\epsilon \quad (3)$$

$$s \cdot \nabla I(r,s) + (k+\sigma_s) I(r,s) = k n^2 \sigma T^4 + \int_{4\pi} I(r,s') \phi(s,s') d\Omega' \quad (4)$$

$$\frac{\partial(\rho Y_i)}{\partial t} + \nabla \cdot (\rho v Y_i) = -\nabla \cdot J_i + R_i + S_i \quad (5)$$

$$K = A e^{\left(-\frac{E_a}{RT}\right)} \quad (6)$$

$$\frac{\boldsymbol{du_p}}{\boldsymbol{dt}} = \frac{\boldsymbol{1}}{\boldsymbol{\tau_p}} \left(\boldsymbol{u} - \boldsymbol{u_p}\right) + \boldsymbol{g} \left(\frac{\boldsymbol{\rho_p - \rho}}{\boldsymbol{\rho_p}}\right) + \boldsymbol{F_{other}} \quad (7)$$

An approximation was made to calculate the calcination of one ton of $CaCO_3$. Assuming that there is no kinetic limitation to the rate of reaction and there is no sensible heat addition, the heat of reaction for calcium carbonate can be used to derive the energy required. The upper bound for the energy required to calcine calcium carbonite is 178 kJ/mol (1778 kJ/kg). 1 ton of CaCO3 would require 1778000 kJ of energy. By assuming a 200 K DT on the steam side which gives a total enthalpy of 9.46 kJ/mol (62.90 - 53.44 kJ/mol using enthalpy tables for steam) (524.8 kJ/kg), the total mass of steam needed to react 1 ton of cement would be 3387 kg. In this study, we are reacting 10 kg/hr. (0.0027 kg/s) of cement in the vessel. This would require a steam flow rate of 0.0094 kg/s. The steam flow rate that the system has at nominal operating conditions is 0.0044 kg/s. Since a much higher DT is used on the steam side, 1200 °C to ~800 °C, about half the calculated flow rate would be needed for the reaction, 0.0045 kg/s.

3. Results and Discussion

There are three main variables that are considered to select the best geometry. Calcination rate, fraction exited, and residence time. The precalciner must calcine as much of the particles as possible, and the particles must reach the bottom of the precalciner. These were ranked from highest to lowest for all cases, and the results for the top five cases are shown are shown in table 2.

Table 2. *Top five ranked cases from highest to lowest calcination rate.*

Case number	Calcination rate	Fraction exited	Mean residence time (s)
13	0.8728	0.6222	1.6011
72	0.7204	0.3933	1.9783
20	0.6931	0.4472	1.9482
114	0.6653	0.4421	1.8318
59	0,6629	0.425	1.7648

Case number 13 had the highest calcination rate, and thus was selected as the best geometry for the precalciner design. The case number 13 precalciner geometry is shown in figure 6, and the geometric dimensions for the precalciner are showed in table 3.

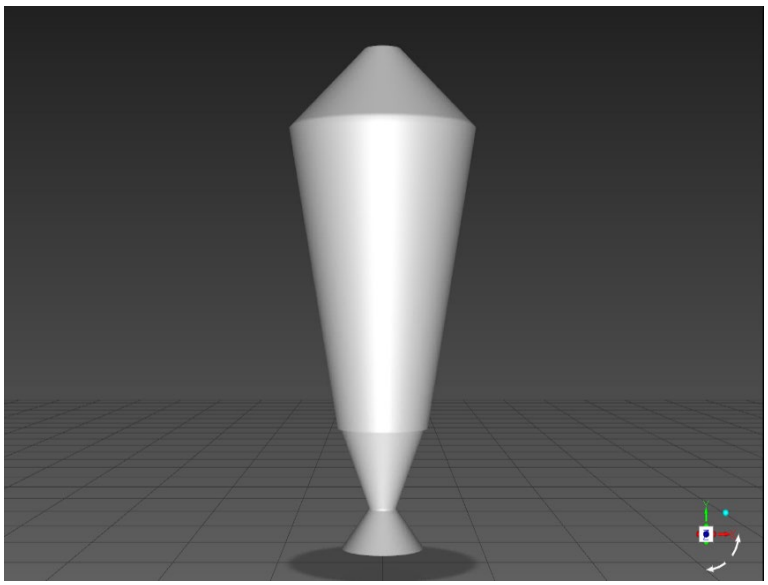

Figure 6. *Case number 13 geometry.*

Table 3. *Case number 13 geometric dimensions.*

Center height	1500 mm.
Center min diameter	500 mm.
Center slope	10◦
Bottom cone height	400 mm.
Bottom cone diameter	150 mm.
Top cone height	400 mm.
Top cone diameter	200 mm.

Although case number 13 ranked the highest of all the cases, the slope made the geometry hard and thus expensive to manufacture. To solve this, the center slope was removed, and a single cylinder-shaped geometry case was created. A new refined mesh was created for both case number 13 and the cylinder-shaped case. The new meshes had 1 million elements each. These cases were simulated, and their results compared in table 4 to determine if the simplified cylinder-shaped geometry would keep close results to the original. The cylinder-shape case proved to have even better results compared to the case number 13 case. The calcination rate, fraction exited, and mean residence time improved from case number 13, making this simplified cylindrical-shape geometry the chosen one for manufacturing. It is important to note that the results from table 3 to 4 change significantly since the mesh from the previous cases was not as refined, and thus causing the difference in the results. The finalized geometry can be seen in figure 7, and the visualization of the particles calcination rate, and residence time can be seen in figure 8.

Table 4. *Cylinder-shape vs case number 13 results.*

	Case Number 13	**Cylinder-Shape Case**
Calcination Rate	0.3958	0.4564
Fraction Exited	0.8736	0.9167
Mean Residence Time (s)	0.7229	0.8253

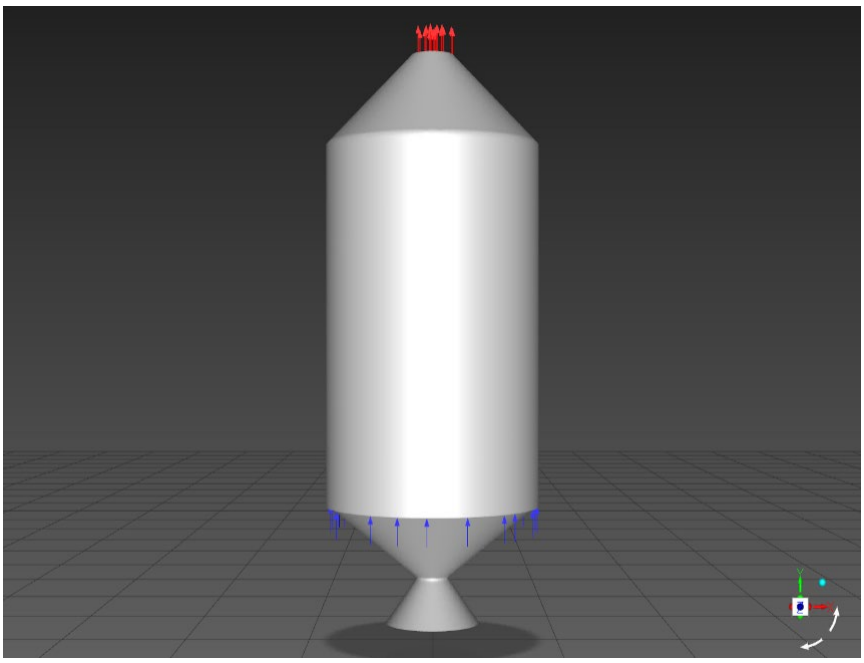

Figure 7. *Finalized precalciner geometry.*

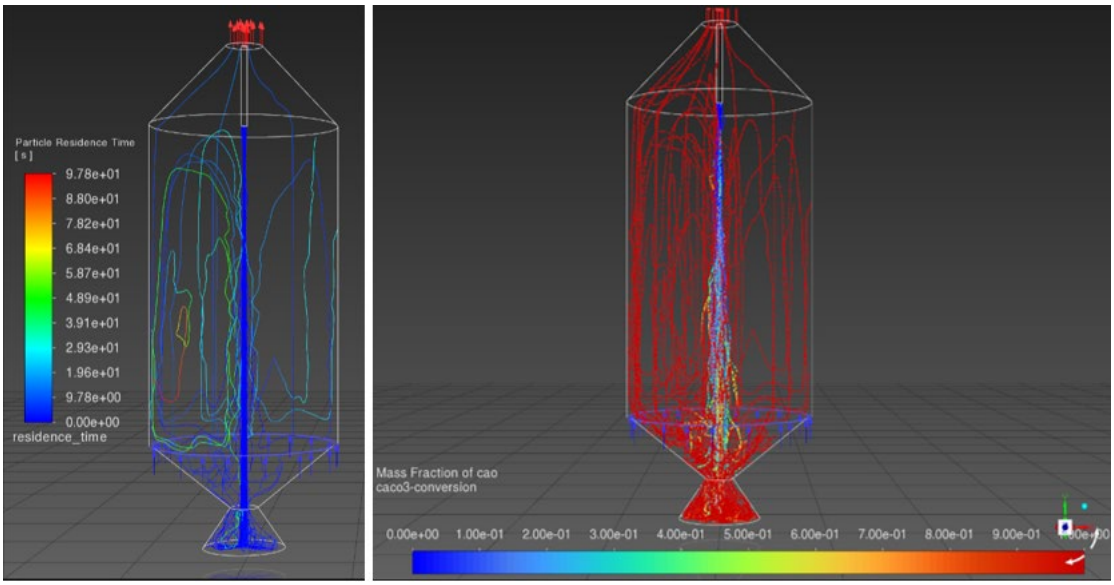

Figure 8. *Particles residence time (left) and calcination rate (right).*

4. Conclusion and Future Work

A geometry optimization study for a precalciner for cement production using a H_2O and CO_2 heat transfer fluid was presented. The geometries were ranked from highest to lowest calcination rate and residence time to determine the best geometry. The geometry was then simplified to reduce complexity and manufacturability. The geometry will now be manufactured and tested to both validate the CFD model, and asses the efficacy of this system.

Data availability statement

Data will be provided upon request.

Author contributions

Javier Martell: Article author, CFD modeling.

Brantley Mills: CFD modeling, Ideation, Optimization Framework creation.

Nathan Schroeder: Project leadership, Ideation.

Competing interests

The authors declare that they have no competing interests.

Funding

This work was funded in part or whole by the U.S. Department of Energy Solar Energy Technologies Office under Award Number 40261. This report was prepared as an account of work sponsored by an agency of the United States Government. Neither the United States Government nor any agency thereof, nor any of their employees, makes any warranty, express or implied, or assumes any legal liability or responsibility for the accuracy, completeness, or usefulness of any information, apparatus, product, or process disclosed, or represents that its use would not infringe privately owned rights. References herein to any specific commercial product, process, or service by trade name, trademark, manufacturer, or otherwise does not necessarily constitute or imply its endorsement, recommendation, or favoring by the United States Government or any agency thereof. The views and opinions of the authors expressed herein do not necessarily state or reflect those of the United States Government or any agency thereof.

Acknowledgement

Sandia National Laboratories is a multimission laboratory managed and operated by National Technology and Engineering Solutions of Sandia, LLC., a wholly owned subsidiary of Honeywell International, Inc., for the U.S. Department of Energy's National Nuclear Security Administration under contract DE-NA0003525.

References

[1] R. M. Andrew, Global CO2 emissions from cement production, Earth Syst. Sci. Data 10 (1), 195-217 (2018).

[2] T. Hanein, Y. Hayashi, C. Utton, M. Nyberg, J.-C. Martinez, N.-I. Quintero-Mora and H. Kinoshita, Pyro processing cement kiln bypass dust: Enhancing clinker phase formation, Construction and Building Materials 259, 120420 (2020).

[3] R. Novis, History of Cement, World Cement Association, cited 2023; Available from: https://www.worldcementassociation.org/aboutcement/ourhistory#:~:text=The%20precursor%20to%20modern%2Dday,then%20mixing%20it%20with%20water.

[4] I. Tiseo, Global CO2 emissions from cement manufacturing 1960-2022, Statistica, [cited 2023; Available from:https://www.statista.com/statistics/1299532/carbon-dioxideemissionsworldwidecementmanufacturing/#:~:text=Global%20CO%E2%82%82%20emissions%20from%20cement%20manufacturing%201960%2D2022&text=Global%20emissions%20from%20the%20manufacture,dioxide%20(MtCO%E2%82%82)%20in%202022.

[5] C. Cormos, Decarbonization options for cement production process: A techno-economic and environmental evaluation, Fuel 320, 123907, (2022).

[6] International Energy Agency – Greenhouse Gas R&D Programme (IEAGHG). Deployment of CCS in the cement industry. Report 2013/19, Cheltenham, UK, 2013.
[7] D. Moore. Cement Plants and Kilns in Britain and Ireland. 2013 [cited 2022; Available from: https://www.cementkilns.co.uk/ckr_therm.html.
[8] R. Cai, Y. Huang, Y. Li, Y. Wu, H. Zhang, M. Zhang, H. Yang and J. Lyu, Effects of the Limestone Particle Size on the Sulfation Reactivity at Low SO2 Concentrations Using a LC-TGA, Materials 12 (9), 1496 (2019).
[9] Precalciner, AGICO Cement, [cited 2023; Available from:https://www.cement-plants.com/clinkerproduction/precalciner/#:~:text=What%20is%20precal-ciner%20in%20cement,is%20necessary%20for%20cement%20plants%3F
[10] Adams, B.M., et al. "Dakota, A Multilevel Parallel Object-Oriented Framework for Design Optimization, Parameter Estimation, Uncertainty Quantification, and Sensitivity Analysis: Version 6.10 User's Manual," Sandia Technical Report SAND2014-4633, July 2014. Updated